journal

J. Am. Ceram. Soc., 84 [5] 962–68 (2001)

Dense Layered Molybdenum Disilicide–Silicon Carbide Functionally Graded Composites Formed by Field-Activated Synthesis

Ellen M. Carrillo-Heian,* R. Douglas Carpenter, Glaucio H. Paulino,† Jeffery C. Gibeling, and Zuhair A. Munir*,‡

Department of Chemical Engineering and Materials Science, University of California, Davis, California 95616

Dense, layered, single- and graded-composition composites of $MoSi_2$ and SiC were formed from elemental powders in one step, using the field-activated pressure-assisted combustion method. Compositions ranging from 100% $MoSi_2$ to 100% SiC were synthesized, with relative densities ranging from 99% to 76%, respectively. X-ray diffractometry results indicated the formation of pure phases when the concentration of $MoSi_2$ was high and the appearance of a ternary phase, $Mo_{4.8}Si_3C_{0.6}$, when the concentration of SiC was high. Electron microprobe analysis results showed the formation of stoichiometric and uniformly distributed phases. A layer-to-layer variation in composition of 10 mol% was sufficient to prevent thermal cracking during formation of the layered functionally graded materials.

I. Introduction

THE existence of phase gradation in nature long has been recognized in such materials as bamboo, bone, and seashell. Bamboo and bone are radially graded structures: dense, tough, and rigid on the outside and soft, light, and flexible on the inside. Synthetic graded materials, generally referred to as functionally graded materials (FGMs), have similar variations in structure, composition, or properties, and have been systematically studied since the mid-1980s.[1] One of the early driving forces for research in FGMs was the development of thermal barrier materials for use in the United States–Japan National Space Plane.[1] FGMs have many thermal applications that are superior to bonded single-phase layers, because the gradual variation in concentration of the two phases can alleviate problems resulting from differences in thermal expansion coefficients, thus minimizing failure due to thermal stress concentration.

Fabricating FGMs offers a technological challenge. Broadly speaking, techniques are classified in two groups: constructive processes, in which two or more components are assembled physically to form a gradient, and transport-based processes, in which heat or mass transfer causes the formation of a gradient.[2] A common and relatively simple constructive method of producing FGMs is stacking and compacting of premixed homogeneous layers. When the variations in concentration between layers are relatively small, the material approaches a continuous composition, and stress concentrations at the interfaces can be decreased to practically insignificant values. Typically, the stacked layers are previously synthesized composites that are subsequently consolidated by sintering at high temperatures. In this article, we report the results of an investigation using a new method: the simultaneous synthesis and densification of FGMs using elemental reactants. The method is constructive, in that we stack layers of reactants to form the gradient. The system investigated is the $MoSi_2$–SiC FGM, because it possesses an easily modeled mechanical behavior and because SiC-reinforced $MoSi_2$ seems to have properties superior to monolithic $MoSi_2$.[3]

$MoSi_2$ is an electrically conducting ceramic that exhibits excellent high-temperature oxidation resistance. Above ~800°C, in air, $MoSi_2$ forms a glassy SiO_2 layer that provides oxidation protection up to ~1700°C,[4] near the softening temperature of the glass. The brittleness at low temperatures and lack of creep resistance at high temperatures of $MoSi_2$ have led to extensive efforts to improve its mechanical properties.[5–7] The potential success of $MoSi_2$ composites in oxidizing and aggressive environments[3] has led to many various reinforcing approaches, including the addition of tantalum, molybdenum, niobium, and niobium–aluminum–titanium alloy as fibers and lamellae[8–10] and niobium and ZrO_2 as particles.[11] The addition of SiC particles to $MoSi_2$ has received particular attention because of early reports of improved room-temperature and high-temperature strength and fracture toughness.[3] Various techniques to add SiC to $MoSi_2$ have been used by several researchers.[12] These techniques include chemical vapor infiltration/deposition,[12] the Martin Marietta XD™ process,[13] plasma spraying,[14] and reactive vapor infiltration,[15] in addition to or in combination with hot-pressing, hot isostatic pressing (HIPing), and sintering.[16] Reactive powder sintering (cosynthesis) starting from Mo_2C and silicon also has been pursued.[17]

The direct synthesis of $MoSi_2$–SiC composites from the elements has been previously investigated by combustion synthesis, with mixed results.[18–20] In recent work, conventional self-propagating high-temperature combustion synthesis (SHS) on layered mixtures as well as simultaneous combustion (thermal explosion) on single-composition mixtures of molybdenum, silicon, and carbon extinguished when the anticipated fraction of SiC was >33 mol%.[19] Mechanical alloying has been used to activate elemental powders before hot pressing at 1650°C and 35–40 MPa for 1 h, resulting in complete combustion in samples with 20 and 40 vol% SiC (33 and 56 mol%).[20] In contrast, electric-field-activated SHS has produced porous composites with compositions ranging from 100 mol% $MoSi_2$ to 100 mol% SiC, with almost no intermediate phases,[18] but with porosity contributions from extrinsic and intrinsic sources.[21] The need to activate the reaction by electric field, milling, preheating, or some other means is dictated by a thermodynamic limitation resulting from a low enthalpy of reaction.[22] The adiabatic combustion temperature, T_a, for $MoSi_2$ is 1942 K and that for SiC is 1851 K.[23] The former is near the limit considered necessary to generate a self-propagating wave. However, that for SiC is lower; thus, reactions to synthesize composites with significant amounts of SiC cannot be self-sustaining and require activation. Field-activated pressure-assisted combustion synthesis provides this activation in the form of current directly applied to the starting powders (if they are conductive) or to the local region in the die around the powders (if they are insulating).

J. J. Petrovic—contributing editor

Manuscript No. 188447. Received August 1, 2000; approved December 20, 2000.
Supported by the National Science Foundation under Grant No. CMS-9713798 (Mechanics and Materials Program).
*Member, American Ceramic Society.
†Current address: Department of Civil and Environmental Engineering, University of Illinois, Urbana, Illinois.
‡Author to whom correspondence should be addressed.

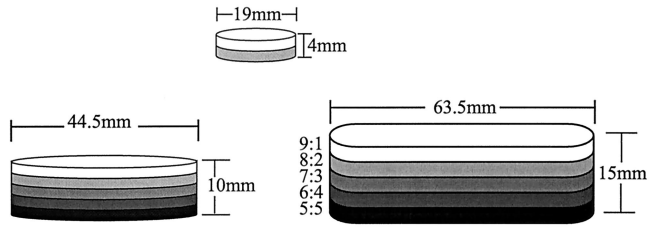

Fig. 1. Sample geometries.

As indicated above, in this article, we report on a new method of forming both FGMs and $MoSi_2$–SiC composites from elemental powders in one step, at nearly full theoretical density. The simultaneous synthesis and compaction are accomplished under the influence of an electric field (current) in a graphite die, combined with uniaxial pressure. The benefit of the field (in reality a current) is believed to be a combination of effects, including providing Joule heat,[24,25] mass-transport enhancement through electromigration,[26] and the possibility of creating a plasma between the contacting powder particles.[27] The use of this method to simultaneously synthesize and densify monolithic materials, including nanometer-sized phases, has been previously demonstrated.[28–30]

II. Experimental Materials and Methods

$MoSi_2$–SiC samples were produced in several geometries over the course of the work, as shown in Fig. 1. Initial studies focused on the synthesis of 19 mm diameter cylinders with heights that varied from 3 to 6 mm. Later, disk-shaped samples 44.5 mm in diameter (height 10 mm) and oblong samples measuring 12.7 mm in width, 63.5 mm in length, and 15 mm in height were used. The latter two geometries were used to produce beams for mechanical testing in three- or four-point bending.

Single-composition composite samples were produced to measure the physical characteristics of the various compositions. Next, two-layer samples were produced to qualitatively assess thermal stress development and layer cohesion, before proceeding to larger and more complex samples. Finally, five-layer graded samples were produced in the two larger sizes for mechanical testing. Five-layer samples were produced in two combinations with 10 mol% increments between adjacent layers within the following limits: 100% $MoSi_2$–60% $MoSi_2$ and 90% $MoSi_2$–50% $MoSi_2$.

The apparatus utilized in this research is the spark plasma sinterer (SPS; Sumitomo Coal Mining Co., Inc., Tokyo, Japan).[27] This machine is a uniaxial 100 kN press combined with a 15 V, 5000 A pulsed direct-current power supply to simultaneously provide current and pressure to a conductive die and sample. The pulse cycle in this work is 12 ms on and 2 ms off. Joule heating of the die and the sample results in the combustion of the sample, and the applied pressure densifies the sample at the same time. A similar apparatus built in our laboratory has been used for some of the experiments: The field-activated pressure-assisted synthesis apparatus (FAPASA) also consists of a 100 kN press and a current source, but the current is 60 Hz alternating-current, with a maximum of 1750 A at 10 V. The SPS can be controlled via a temperature controller or manually by current, whereas the FAPASA has only manual current control. In both machines, temperature is measured on the surface of the die using a pyrometer. The SPS also has computer data collection of the voltage, current, load applied, temperature, displacement (shrinkage), and displacement rate. The FAPASA displays voltage, current, and temperature, but has no recording capability. In this case measurements are recorded manually every 30 s.

Elemental powders of molybdenum, silicon, and carbon were used in this work. Information on these starting powders is given in Table I. Powders were mixed in stoichiometric proportions according to the following equation:

$$x\mathrm{Mo} + (1 + x)\mathrm{Si} + (1 - x)\mathrm{C} \rightarrow x\mathrm{MoSi_2} + (1 - x)\mathrm{SiC}$$

The mole fraction of molybdenum (x) and, thus, $MoSi_2$ was varied from 0.0 to 1.0 in 10% increments. The powders were mixed via either a turbula mixer for 1 h or a rolling mill for 24 h, in both cases using 7 mm diameter zirconia-stabilized tetragonal-alumina balls with no solvent. To form a single-composition composite sample, the appropriate quantity of mixed powder was weighed and poured into a graphite die lined with graphite foil, and cold-pressed at 13.344 N (3000 lb, 48 MPa for the small dies). To form an FGM, each layer was weighed, poured into the graphite-foil-lined die, tapped to level, then pressed by hand. The punch was then removed and the next layer was poured into the die and treated similarly, until all five layers were in the die. The assembly was then cold-pressed at 13.344 N and treated identically to the single-composition composite samples. The dies used were three-piece dual-action dies machined from EDM-grade graphite. The dies were used repeatedly until they broke.

After the samples were packed, they were reacted in either the SPS or the FAPASA, under a load that varied with the sample size and the machine. Samples reacted in the FAPASA were 19 mm in diameter and were subjected to a pressure of 95 MPa. The samples reacted in the SPS were subjected to a pressure of 63 MPa if they were 19 mm, but 25 MPa if they were either of the other two sizes. The decrease in pressure for the larger samples was necessary to prevent breakage of the larger dies because of increased hoop stress in the die walls. The typical sample reacted in the FAPASA was maintained at 1750 A for 10 min. In specific instances, different times were used, as discussed below. In the SPS, the heating cycle was controlled based on the temperature. The general pattern was to heat the sample to 1200° or 1300°C steadily, and then furnace cool. The control of the temperature in the larger dies was not very stable, resulting in fluctuations.

There was a substantial thermal mass involved in the die–sample system, which was different for the large samples and the small samples. The thermal mass translated to a delay between the application of current and the corresponding increase of temperature on the outside of the die. This thermal delay was expected to vary with the thickness and diameter of the graphite die, as well as the reactant-packing and surface characteristics. For a given current, the voltage and, thus, the temperature varied with the resistance of each system. This resistance also varied with the amount of silicon and carbon in the sample and the exact packing conditions; therefore, it was not possible to keep the resistance constant. Samples with resistances that were atypical were discarded.

Each sample was removed from the die when the reaction was complete and was lightly ground to remove the graphite foil. Samples were sectioned from the as-pressed disks using a low speed (400 rpm) saw with a diamond blade. Cross-sectioned samples were ground flat for X-ray diffractometry (XRD) or mounted in epoxy and diamond polished to a 1 μm finish for microscopy.

Table I. Properties of Starting Powders

Material	Source	Particle-size classification	Purity (%)
Molybdenum	Alfa Aesar (Ward Hill, MA)	3–7 μm	99.95
Silicon	Alfa Aesar	−325 mesh	99.5
Graphite carbon	Asbury Graphite Mills (Asbury, NJ)	0.6 μm (average)	99

The resulting samples were characterized using XRD with Cu*K*α radiation for bulk phase identification. Mounted and polished samples were examined using scanning electron microscopy (SEM) and optical microscopy for phase distribution, and electron microprobe analysis (EPMA) was used for chemical species distribution and interface sharpness. EPMA was used to collect back-scattered electron (BSE) images and X-ray dot maps for Mo*L*α and Si*K*α wavelengths at magnifications of 500× and 1000×. A 1 μm spot size at 20 kV and 10 nA was used for analysis of the phases present. Density was measured via geometric and Archimedes (submersion in methanol) methods.

Finally, large single-composition beams were cut using a diamond saw and were ground to final size on wet, 240 grit SiC paper. Small strain gauges were glued to the beams in axial and transverse orientations in preparation for mechanical testing. The beams were loaded in four-point bending to measure Young's modulus (axial strain) and Poisson's ratio (transverse strain).

III. Results

The reaction of molybdenum and silicon to form $MoSi_2$ in this work is always marked by an abrupt compaction event, usually audible and always accompanied by an abrupt decrease in resistance. This is believed to be the consequence of a combustion reaction between the powders. This event happens at a fairly consistent exterior temperature of ~1100°C in the SPS. Other researchers have reported this compaction event as well,[31] occurring at 1050°C in a similar SPS experimental setup treating molybdenum and silicon to form $MoSi_2$. The magnitude of the compaction decreases with increasing SiC. Products of experiments in which the current is turned off immediately after the compaction contain the desired phases but are not microstructurally as homogeneous as samples held at temperature for a few minutes after compaction.

XRD reveals that the reactions are always complete, with another phase appearing as the concentration of carbon increases. The third phase is $Mo_{4.8}Si_3C_{0.6}$, a so-called Nowotny phase, that has been reported by several researchers.[32] It is hexagonal, with space group $P6_3/mcm$, and it is stable down to room temperature, as reported by Parthé *et al.*[33] Figure 2 shows XRD patterns for three composite samples in which $x = 0.3$, 0.5, and 0.8. Figure 2 shows the relative abundance of the third phase as a function of carbon content. As the amount of carbon in the reactants increases, the amount of $Mo_{4.8}Si_3C_{0.6}$ increases. When $x = 0.8$, there is little evidence of the presence of this carbosilicide, as shown in the small peaks in the 2θ range of 42°–44°. These peaks increase slightly as x decreases to 0.5 and become significant when $x = 0.3$.

The density of the resulting $MoSi_2$–SiC composites was measured for each composition. Density ranged from 76% to 98.6% of the theoretical density, showing a dependence on composition as x decreased from 1.0 to 0.2, as shown in Fig. 3. Initially, the density decreased relatively slowly as the amount of SiC was increased to $x = 0.5$, and then decreased at a much higher rate beyond this composition. In the range of $x < 0.4$, the density was <92%, a value considered too low for subsequent mechanical characterization. For this reason, only FGM samples with a minimum $MoSi_2$ content of 50 mol% were subsequently made and investigated. The theoretical density was calculated based only on the nominal mole fractions of $MoSi_2$ and SiC in the product, excluding $Mo_{4.8}Si_3C_{0.6}$, because the quantity of $Mo_{4.8}Si_3C_{0.6}$ in each sample was unknown. The inclusion of $Mo_{4.8}Si_3C_{0.6}$ in the calculation would have decreased the sample relative density, because $Mo_{4.8}Si_3C_{0.6}$ was denser than either $MoSi_2$ or SiC. Therefore, in samples with high SiC content, the true density was even lower than that reported. When the SiC content was low, there was little $Mo_{4.8}Si_3C_{0.6}$, and, thus, the error was minimized. Moreover, in samples with high SiC content, it was often observed that a spatial density gradient was present. This was especially obvious in the large oblong samples. A ring of porosity with a denser core was the typical structure observed. Corners were sometimes more dense than the porous ring. This ring might have been due to different reaction rates and pressures at the center and outside of a compact.

Figures 4(a)–(f) represent a set of EPMA images for a bilayer sample. Figures 4(a)–(c) are of the side in which $x = 0.7$, while Figs. 4(d)–(f) are of the side in which $x = 0.3$. Figures 4(a) and (d) are BSE images, Figs. 4(b) and (e) are X-ray dot maps for molybdenum at its *L*α wavelength, and Figs. 4(c) and (f) are dot maps of silicon at its *K*α wavelength. Carbon was not visible using this instrument because of the lack of an appropriate diffracting and focusing crystal. Table II lists the compositions of several spots in the images. Because carbon could not be directly measured, its presence was assumed when the total mass detected did not add up to ~100%. In these situations, it was assumed that the carbon was present in an atomic amount equal to silicon, and the totals were recalculated. If the weight total was now ~100%, then the silicon present at that spot was in SiC. If the weight total was not ~100%, then the assumption that the carbon present was equal in amount to silicon was not a good assumption, and the phase present, therefore, was not SiC. This technique worked quite well for SiC and $MoSi_2$, but did not allow us to distinguish between

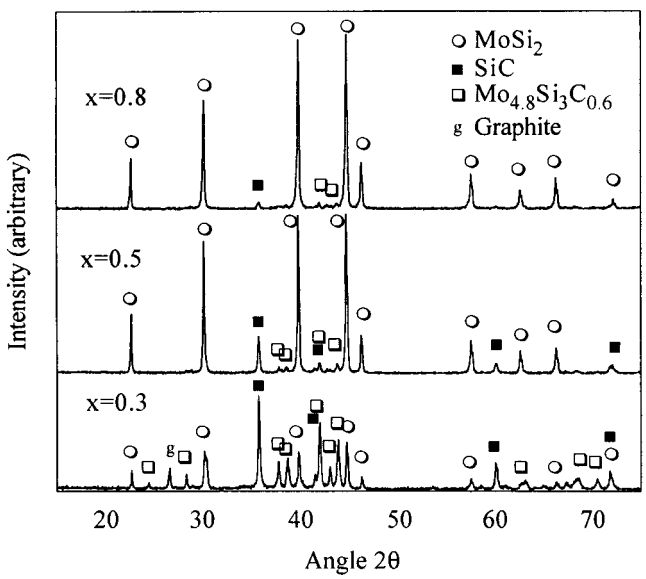

Fig. 2. XRD patterns for three single-composition samples showing $MoSi_2$, SiC, and $Mo_{4.8}Si_3C_{0.6}$: (a) $x = 0.8$, almost no SiC is visible; (b) $x = 0.5$, SiC, $MoSi_2$, and $Mo_{4.8}Si_3C_{0.6}$ are visible; and (c) $x = 0.3$, a large amount of $Mo_{4.8}Si_3C_{0.6}$ is visible.

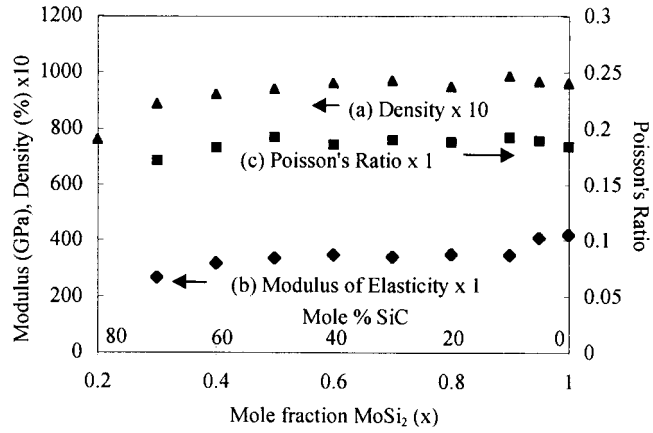

Fig. 3. Plot of (a) density, (b) modulus of elasticity, and (c) Poisson's ratio versus mole fraction of $MoSi_2$ and SiC content for several single-composition samples. All are large oblong samples reacted under a pressure of 25 MPa. Density is plotted as percent of theoretical multiplied by 10.

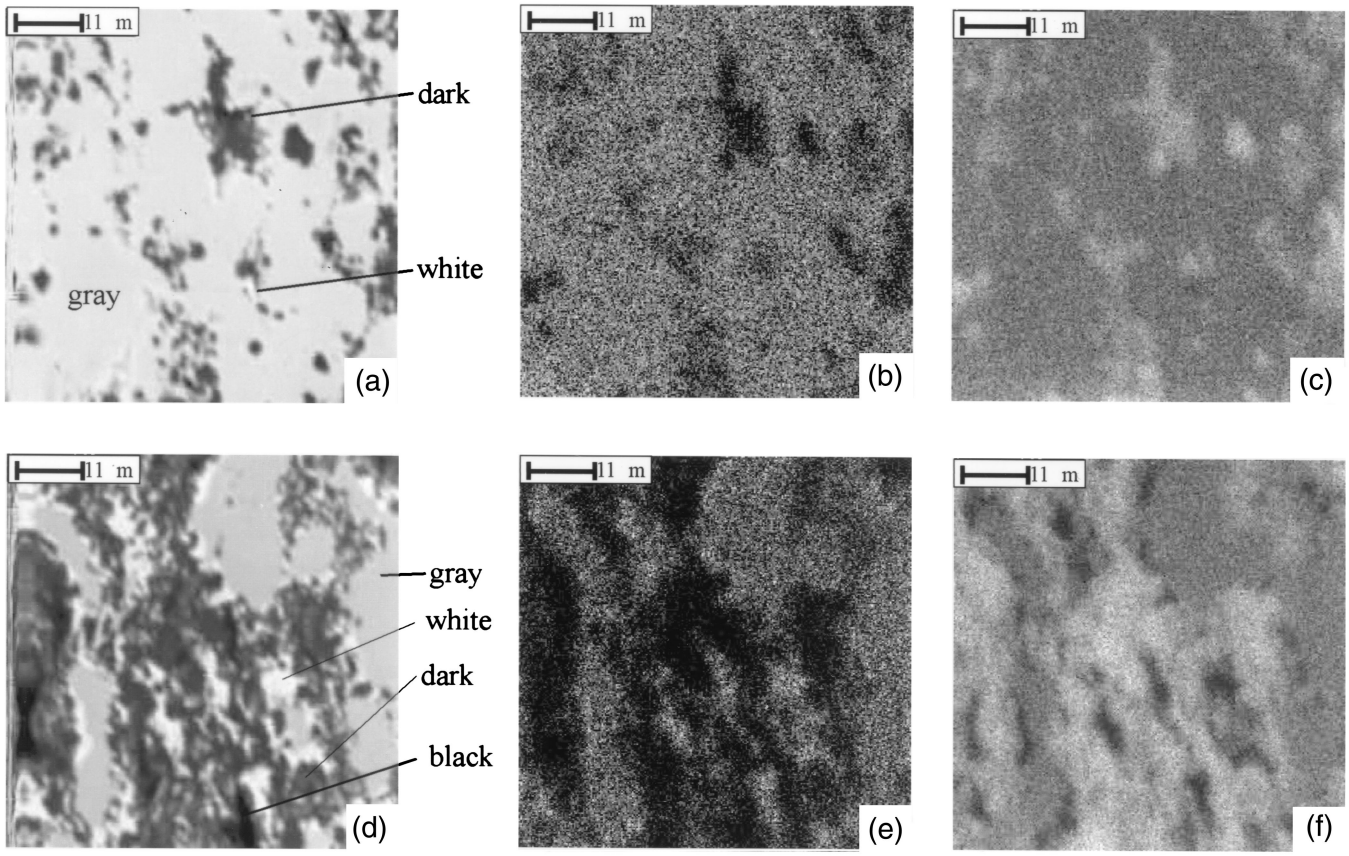

Fig. 4. EPMA images of a bilayer sample for which (a)–(c) $x = 0.7$ and (d)–(f) $x = 0.3$: (a) BSE image showing dark SiC, gray $MoSi_2$, and a very small amount of $Mo_{4.8}Si_3C_{0.6}$; (b) Mo*L*α X-ray dot map; (c) Si*K*α X-ray dot map; (d) BSE image showing black pore, dark SiC, gray $MoSi_2$, and bright $Mo_{4.8}Si_3C_{0.6}$; (e) Mo*L*α X-ray dot map; and (f) Si*K*α X-ray dot map.

Table II. Composition of Several Points in Fig. 4

	Composition (wt%)†				Composition (at.%)†				
	Molybdenum	Silicon	Carbon	Total	Molybdenum	Silicon	Carbon	Total	Phase
$MoSi_2$ rich side, $x = 0.7$									
Dark	23.11	51.67	22.10	96.88	6.15	46.93	46.93	100	SiC
SiC rich side, $x = 0.3$									
Black	11.94	53.92	23.06	88.92	3.14	48.43	48.43	100	Pore
Dark	9.90	64.61	27.63	102.14	2.19	48.90	48.90	100	SiC
Gray	66.09	37.54	0	103.63	34.01	65.99	0	100	$MoSi_2$
White	74.25	26.35	0	100.6	54.80	45.20	0	100	Mo_5Si_3 or $Mo_{4.8}Si_3C_{0.6}$

†By calculation.

Mo_5Si_3 and $Mo_{4.8}Si_3C_{0.6}$, because there was carbon in $Mo_{4.8}Si_3C_{0.6}$ but not in an amount equal to silicon. However, EDS measurements performed on a 50% $MoSi_2$ sample in another SEM photograph confirmed the presence of carbon in the white phase.[2]

A comparison of Figs. 4(a) and (d) shows that the gray phase is far more plentiful in the $x = 0.7$ side than in the $x = 0.3$ side. The gray phase is $MoSi_2$, as shown in Table II. There is almost no white phase in Fig. 4(a), and much white phase in Fig. 4(d). The white phase is either Mo_5Si_3 or $Mo_{4.8}Si_3C_{0.6}$, as shown in Table II. XRD identifies this phase as $Mo_{4.8}Si_3C_{0.6}$, as expected when the concentration of carbon is high. The white phase is quite low in silicon, as shown in Fig. 4(f). Two darker phases are visible in Fig. 4(d): The darker, labeled "black" in the table, yields bad counting statistics (low total weight percent) and, thus, is a pore, while the slightly lighter one, labeled "dark," is the expected SiC phase.

Figure 5(a) is a BSE image of a bilayer sample in which $x = 0.7$ in the top layer and $x = 0.3$ in the bottom layer, showing the interface and the three phases present: "gray" is $MoSi_2$, "dark" is SiC, and "white" is $Mo_{4.8}Si_3C_{0.6}$. The interface between the layers is quite distinct, with no voids or cracks. Two-layer samples in which the difference in composition is >10 mol%, such as this one, usually crack on removal from the graphite die, presumably because of stresses resulting from the difference in CTEs of $MoSi_2$ and SiC. At 1200°C, the CTE of $MoSi_2$ is 1.02 and that of SiC is 0.62, a 40% difference.[34] The cracks that appear in the two-layer samples are generally radial, and, as predicted by the large CTE of $MoSi_2$, form in the $MoSi_2$-rich side. Figure 5(b) is an optical micrograph of cracks in a sample of the same composition as Fig. 5(a), i.e., $x = 0.7$ and $x = 0.3$. The cracks are vertical, as is consistent with thermal shrinkage cracks, and, although one runs across the interface into the SiC-rich side, no cracks run along the interface. A linear rule of mixtures has been used to calculate the CTE at 1200°C for the two layers: the $MoSi_2$-rich layer has a CTE of 0.90 and the SiC-rich layer has a CTE of 0.74. Layers that are 10% different in composition vary in CTE by only ~3%. When the difference in composition between two layers is 10 mol%, no cracks are observed.

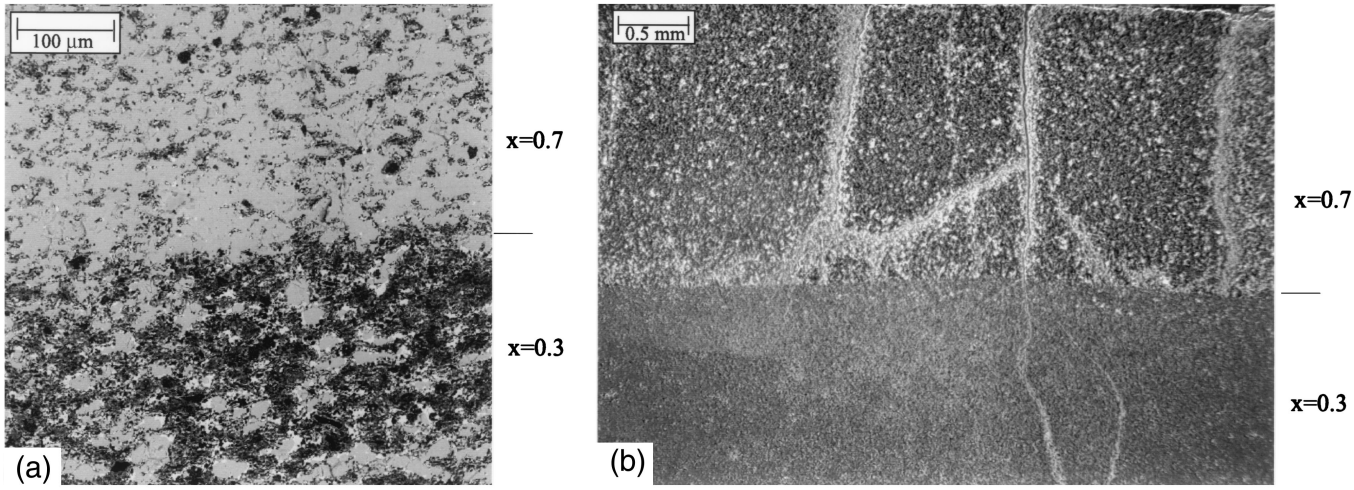

Fig. 5. Two samples in which the top layer is 70% $MoSi_2$ and the bottom layer is 30% $MoSi_2$: (a) BSE image of the interface between two layers, showing good integrity, and (b) optical image showing cracks in the $MoSi_2$-rich layer and one through-crack.

Composition profiles across layer interfaces, such as that shown in Fig. 6, where the two layers are $x = 0.5$ and $x = 0.9$, show an abrupt change at the interface with no composition smoothing under the conditions of these experiments. The approximate thickness of the interface region is 200 μm, or two data points. Figure 6 shows two scans across the interface, one taken near the middle of the sample and the other near the edge. The former is in better agreement with the nominal composition profile, shown as a solid line. The concentrations measured near the edge are somewhat lower (by ~0.5–1.0 at.% silicon). The small loss of silicon is likely the result of interaction with the graphite. There is more scatter on the $x = 0.5$ side as a result of the random distribution of SiC grains: Because there is more SiC on this side, the distribution is less narrow.

To explore the effect of processing time on the interface composition, a series of two-layer samples with compositions of $x = 0.7$ and $x = 0.3$ was held in the FAPASA for 5, 10, 15, and 20 min under a constant current of 1750 A during synthesis. The samples show slight differences in grain size and morphology but are within the limits of the data scatter; no difference in the concentration profile at the interface is evident. All show a step change in concentration.

Figure 7 is an optical image of the cross section of a five-layer FGM, with layer compositions varying from 90% $MoSi_2$ to 50% $MoSi_2$. There is some porosity near the surface of the sample, in the $x = 0.5$ layer, which appears as another layer. This layer has been designed to be thicker than the others, so the porous portion could be cut off and not used in mechanical testing samples. A small region is similarly visible on the $x = 0.9$ surface. Although not visible in this photograph, there is often a small amount of porosity between the $x = 0.6$ and $x = 0.7$ layers, appearing at the interface. However, no thermal cracks are evident. Figure 8 shows the composition profile of a five-layer FGM, with layer compositions varying from 100 to 60 mol% $MoSi_2$. Also included in Fig. 8 are BSE micrographs for each layer, showing the distribution of SiC in the $MoSi_2$ matrix. The 100% $MoSi_2$ layer has a little more scatter than the other layers; this is because the grain size of this layer is so large that the polishing process leads to pullouts and some pitting of the surface, leading to poor counting statistics and larger scatter in the measured data. This abnormal grain growth in the pure $MoSi_2$ layer has led us to make FGMs with compositions ranging from 90% to 50% $MoSi_2$, instead of 100% to 60% for the mechanical-testing samples. The presence of SiC seems to reduce grain growth in the $MoSi_2$, although this effect has not been quantified in this work.

The modulus of elasticity and Poisson's ratio have been measured in single-composition oblong samples and plotted versus concentration of SiC in Fig. 3 along with the sample density. The modulus decreases as the SiC content increases from 0% to 10%, then remains constant until the SiC content reaches 50%. Above 50% SiC, the modulus decreases noticeably with increasing SiC content. The initial decrease in modulus from 5% to 10% SiC is

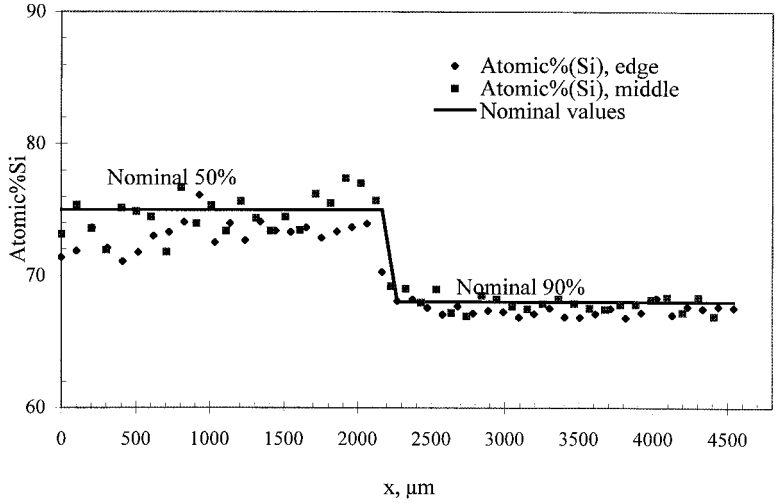

Fig. 6. Composition profile of a bilayer sample with $x = 0.5$ in one layer and $x = 0.9$ in the other.

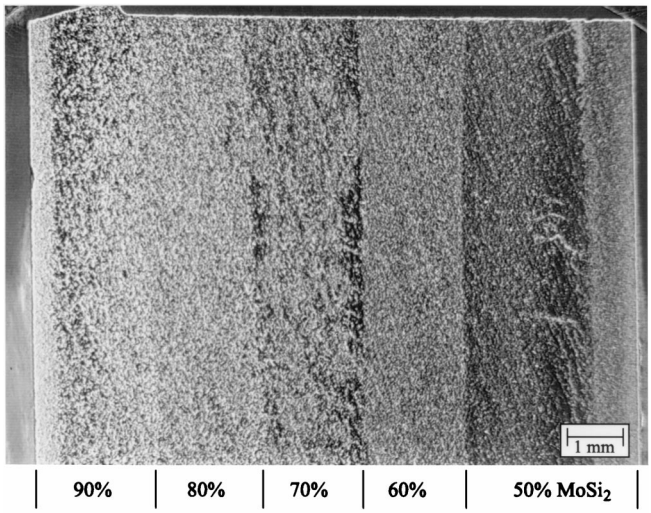

Fig. 7. Optical image of a five-layer FGM in which concentrations varies from $x = 0.9$ to $x = 0.5$.

possibly due to a grain-boundary layer of an intermediate phase, such as $Mo_{4.8}Si_3C_{0.6}$, that is not continuous at 5% SiC but is continuous on the grain boundaries at 10% and higher SiC compositions. Poisson's ratio is constant across the range of compositions from 0% to 50% SiC and then decreases slightly at 60% and 70% SiC because of the decrease in material density. Above 20% SiC, the modulus of elasticity, Poisson's ratio, and the density correlate very well. The linear rule of mixtures predicts an increase in Young's modulus from 0% SiC toward 100% SiC based on literature values of 405 GPa for $MoSi_2$ (sintered) and 470 GPa for SiC (~5% porosity),[35] which disagrees with our results. These values are quite sensitive to processing technique and are unavailable in the literature for materials made via this process. Unfortunately, we have been unable to make fully dense SiC to compare to the literature value and provide an endpoint for a rule of mixtures calculation based on $MoSi_2$ and SiC made by us.

IV. Discussion

The results of this study demonstrate that the imposition of pressure and electric field simultaneously can make feasible the formation of dense $MoSi_2$–SiC composites and layered FGMs. The advantages are simplicity of sample preparation, robustness of the interfaces, and short processing time, as less than an hour of heating is required. The formation of the third phase when the concentration of carbon is high is not necessarily a detriment in this material. A small amount of Mo_5Si_3 is commonly present at the grain boundaries of $MoSi_2$ made by conventional means and is often considered desirable in increasing the ductility of this brittle ceramic. The presence of $Mo_{4.8}Si_3C_{0.6}$ in small quantities may well serve a similar role in reinforcing the FGM.

The presence of porosity in the lower $MoSi_2$ concentration samples (~50 mol% and lower) is a phenomenon observed by other researchers as well.[36] Their studies have involved adding SiC whiskers to $MoSi_2$ and then HIPing. They have suggested that the dominant mechanism for densification in these samples is power-law creep, which means that higher pressures should lead to higher densities. However, in our case, most of the compaction occurs during the chemical reaction; therefore, the power-law creep mechanism is probably not dominant. During the compaction event, a pure SiC sample lost 65% of its final height. The theoretical shrinkage during the reactions to form $MoSi_2$ and SiC from the elements is ~39%, such that 26% of the total height is lost because of porosity reduction. The final density of this sample is 87.5%. Furthermore, a sample of SiC reacted at 63 MPa has the same final density as one reacted at 95 MPa. $MoSi_2$ undergoes a ductile to brittle transition at ~1000°C; therefore, it might be fairly ductile and more easily compacted at the temperatures of this study. However, SiC does not undergo a similar transition. Perhaps this contributes to its lack of compaction.

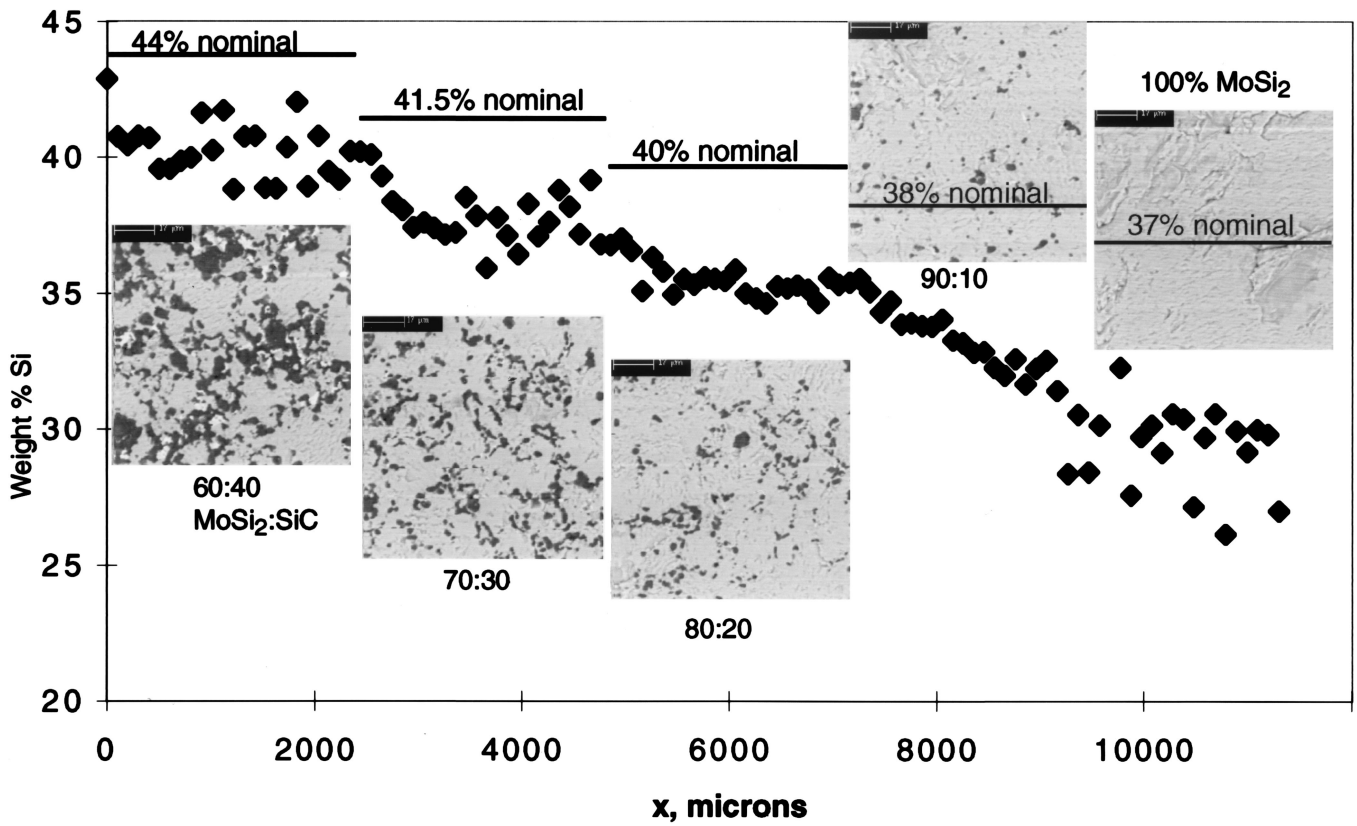

Fig. 8. Composition profile and BSE images of the five layers in an FGM.

No smoothing of the interfaces between layers is evident. This is partly due to the solid nature of the reaction products, as well as the lack of a large concentration difference in a liquid phase, which can act as a driving force for bulk motion of such a phase during the reaction. Two processes by which a component can move from one layer to another are liquid capillary impregnation and diffusion; the former process dominates at the time scale under consideration. The time required for significant diffusion to take place is orders of magnitude greater than the length of time during which these samples are hot. Capillary impregnation is quite likely to occur in SHS; however, in our work, pressure is applied throughout the reaction, so that voids that form in the sample due to shrinkage and expelled gases should be rapidly collapsed, with no time for impregnation. Moreover, the only liquid phase present at any time is silicon, and it is present only as a transient phase. Finally, the concentration of silicon does not vary significantly from layer to layer; therefore, the driving force for the motion of silicon is quite small. The four samples that are held at temperature for various times would be expected to show a variation in interface smoothness if a mechanism faster than solid-state diffusion is operating.

V. Conclusions

The feasibility of forming dense, layered, functionally graded $MoSi_2$–SiC composites by a field-activated pressure-assisted method using an SPS apparatus has been demonstrated. Attention has been paid to the thermal stresses that develop between layers, but the compositional variations between layers can be easily tailored to prevent thermal cracking. Increments of 10 mol% are sufficiently small to prevent thermal cracking in this system. The interfaces between $MoSi_2$ and SiC as well as those between layers of different composition are very robust: Cracking across the interfaces is far more likely than cracking along the interfaces. A third phase, $Mo_{4.8}Si_3C_{0.6}$, is formed when the concentration of carbon is high. A decrease in density with a decrease in $MoSi_2$ concentration is observed, which leads to a decrease in Young's modulus and Poisson's ratio, as observed in single-composition samples. No smoothing of the interfaces between layers is evident within the processing regime explored in this work. Direct extension of this work includes fracture testing of $MoSi_2$–SiC FGMs under three-point bending and development of a finite-element model for $MoSi_2$–SiC FGMs. The authors are currently pursuing this work.

References

[1]A. Mortensen and S. Suresh, "Functionally Graded Metals and Metal–Ceramic Composites: Part 1, Processing," *Int. Mater. Rev.*, **40,** 239–65 (1995).

[2]E. M. Carrillo-Heian, "Simultaneous Synthesis and Densification of Functionally Graded Silicide Composites"; Ph.D. Dissertation. University of California, Davis, 2000.

[3]A. K. Vasudévan and J. J. Petrovic, "A Comparative Overview of Molybdenum Disilicide Composites," *Mater. Sci. Eng.*, **A155,** 1–17 (1992).

[4]G. Sauthoff, *Intermetallics*; p. 114. VCH Verlagsgesellschaft, Weinheim, Germany, 1995.

[5]S. Maloy, A. H. Heuer, J. Lewandowski, and J. J. Petrovic, "Carbon Additions to Molybdenum Disilicide: Improved High-Temperature Mechanical Properties," *J. Am. Ceram. Soc.*, **74,** 2704–706 (1991).

[6]S. Maloy, J. J. Lewandowski, A. H. Heuer, and J. J. Petrovic, "Effects of Carbon Additions on the High-Temperature Mechanical Properties of Molybdenum Disilicide," *Mater. Sci. Eng.*, **A155,** 159–63 (1992).

[7]U. V. Waghmare, V. Bulatov, E. Kaxiras, and M. S., Duesbery, "Microalloying for Ductility in Molybdenum Disilicide," *Mater. Sci. Eng.*, **A261**, 147–57 (1999).

[8]T. C. Lu, A. G. Evans, R. J. Hecht, and R. Mehrabian, "Toughening of $MoSi_2$ with a Ductile (Niobium) Reinforcement," *Acta Metall. Mater.*, **39**, 1853–62 (1991).

[9]F. Ye, R. J. Lederich, and W. O. Soboyejo, "An Investigation of the Fatigue and Fracture Behavior of Laminated $MoSi_2$/Nb·15Al·40Ti Composites"; pp. 457–72 in *Deformation and Fracture of Ordered Intermetallic Alloys III*. Edited by W. O. Soboyejo, T. S. Strivatsan, and H. L. Fraser. The Materials Society, Warrendale, PA, 1996.

[10]W. O. Soboyejo, F. Ye, L.-C. Chen, N. Bahtishi, D. S. Schwartz, and R. J. Lederich, "Effects of Reinforcement Architecture on the Fatigue and Fracture Behavior of $MoSi_2$/Nb Composites"; pp. 359–90 in *Fatigue and Fracture of Ordered Intermetallic Materials II*. Edited by W. O. Soboyejo, T. S. Srivatsan, and R. O. Ritchie. The Materials Society, Warrendale, PA, 1995.

[11]I. J. Shon and Z. A. Munir, "The Synthesis of $MoSi_2$– *x*Nb and $MoSi_2$– *y*ZrO_2 Composites by Field-Activated Combustion Methods," *Mater. Sci. Eng. A*, **A202**, 256–61 (1995).

[12]N. S. Stoloff, "An Overview of Powder Processing of Silicides and Their Composites," *Mater. Sci. Eng. A*, **A261,** 169–80 (1999).

[13]C. R. Feng and D. J. Michel, "Microstructures of XD™ $MoSi_2$ + SiC_p Composites"; pp. 1051–56 in *High-Temperature Ordered Intermetallic Alloys V*. Edited by I. Baker, R. Darolia, J. D. Whittenberger, and M. H. Yoo. Materials Research Society, Pittsburgh, PA, 1993.

[14]Y.-L. Jeng, E. J. Lavernia, J. Wolfenstine, D. E. Bailey, and A. Sickinger, "Creep Behavior of Plasma-Sprayed SiC-Reinforced $MoSi_2$," *Scr. Metall. Mater.*, **29,** 107–11 (1993).

[15]N. Patibandla, W. B. Hillig, M. R. Ramakrishnan, D. E. Alman, and N. S. Stoloff, "*In Situ* Processing of $MoSi_2$-Based Composites"; pp. 59–69 in *High-Temperature Silicides and Refractory Alloys Symposium*, Materials Research Society Symposium Proceedings, Vol. 322. Edited by C. L. Briant, J. J. Petrovic, B. P. Bewlay, A. K. Vasudévan, and H. A. Lipsitt. Materials Research Society, Pittsburgh, PA, 1994.

[16]J. M. Ting, "Sintering of Silicon Carbide/Molybdenum Disilicide Composites Using Boron Oxide as an Additive," *J. Am. Ceram. Soc.*, **77,** 2751–52 (1994).

[17]C. H. Henager Jr., J. L. Brimhall, and J. P. Hirth, "Synthesis of a $MoSi_2$–SiC Composite *in Situ* Using a Solid-State Displacement Reaction," *Mater. Sci. Eng. A*, **A155**, 109–14 (1992).

[18]S. Gedevanishvili and Z. A. Munir, "An Investigation on the Combustion Synthesis of $MoSi_2$– β-SiC Composites through Electric Field Activation," *Mater. Sci. Eng. A*, **A242,** 1–6 (1998).

[19]K. Monroe, S. Govindarajan, J. J. Moore, B. Mishra, D. L. Olson, and J. Disam, "Combustion Synthesis of $MoSi_2$ and $MoSi_2$ Composites"; see Ref. 15, pp. 113–18.

[20]S. Jayashankar, S. E. Riddle, and M. J. Kaufman, "Synthesis and Properties of *in Situ* $MoSi_2$/SiC Composites"; see Ref. 15, pp. 33–40.

[21]Z. A. Munir, "Analysis of the Origin of Porosity in Combustion-Synthesized Materials," *J. Mater. Synth. Process.*, **1**, 387–94 (1993).

[22]Z. A. Munir, "Field Effects in Self-Propagating Solid-State Reactions," *Z. Phys. Chem.*, **207**, 39–57 (1998).

[23]HSC Chemistry for Windows v. 4.0 Software Package, Outokumpu Research Oy Information Service, Pori, Finland, 1999.

[24]A. Feng and Z. A., Munir, "The Effect of an Electric Field on Self-Sustaining Combustion Synthesis, Part I: Modeling Studies," *Metall. Trans.*, **26B**, 581–86 (1995).

[25]A. Feng and Z. A. Munir, "The Effect of an Electric Field on Self-Sustaining Combustion Synthesis, Part II: Field-Assisted Synthesis of β-SiC," *Metall. Trans.*, **26B**, 587–93 (1995).

[26]N. Bertolino, J. Garay, U. Anselmi-Tamburini, and Z. A. Munir, "Electromigration Effects in Al–Au Multilayers," *Scr. Mater.*, in press.

[27]M. Tokita, "Development of Large-Size Ceramic/Metal Bulk FGM Fabricated by Spark Plasma Sintering," *Mater. Sci. Forum*, **308–311**, 83–88 (1999).

[28]Z. A. Munir, I. J. Shon, and K. Yamazaki, "Simultaneous Synthesis and Densification by Field-Activated Combustion," U.S. Pat. No**.** 5 794 113, Aug. 11, 1998.

[29]I. J. Shon, Z. A. Munir, K. Yamazaki, and K. Shoda, "Simultaneous Synthesis and Densification of $MoSi_2$ by Field-Activated Combustion," *J. Am. Ceram. Soc.*, **79,** 1875–80 (1996).

[30]Z. A. Munir, F. Charlot, F. Bernard, and E. Gaffet, "One-Step Synthesis and Consolidation of Nanomaterials," U.S. Pat. Application No. 9 374 049, Aug. 13, 1999.

[31]T. Y. Um, Y. H. Park, H. Hashimoto, S. Sumi, T. Abe, and R. Watanabe, "Fabrication of Mo-Si System Intermetallic Compounds by Pulse Discharge Pressure-Combustion Synthesis," *Powder Powder Technol.*, **44**, 530–34 (1997).

[32]P. Villars, A. Prince, and H. Okamoto, *Handbook of Ternary Alloy Phase Diagrams*; pp. 7068–72. ASM International, Materials Park, OH, 1995.

[33]E. Parthé, W. Jeitschko, and V. Sadagopan, "A Neutron Diffraction Study of the Nowotny Phase Mo_5Si_3C," *Acta Crystallogr*, **19,** 1031–37 (1965).

[34]Y. S. Touloukian, *Thermophysical Properties of High-Temperature Solid Materials*; pp. 129 and 441. Macmillan, New York, 1967.

[35] M. Bauccio (Ed.), *ASM Engineering Materials Reference Book*, 2nd ed.; p. 214. ASM International, Materials Park, OH, 1994.

[36]S. M. L. Sastry, R. Suryanarayanan, and K. L. Jerina, "Consolidation and Mechanical Properties of $MoSi_2$-Based Materials," *Mater. Sci. Eng. A*, **A192/193,** 881–90 (1995). □